Coupled Thermal-Electromagnetic Model for Microwave Heating of Temperature-Dependent Dielectric Media

Yaron Alpert and Eli Jerby

***Abstract*— Microwave heating processes involve electromagnetic and thermal effects coupled together through the local temperature dependence of the material dielectric properties. This paper presents a one-dimensional model for the coupled electromagnetic-thermal process and demonstrates its solutions for typical problems. The local temperature dependence of the lossy dielectric medium is taken into account in two different time scales. One is the heat-generation time scale due the microwave radiation, and the other is the temperature diffusion time scale. The two time-scale approach minimizes the computation time and provides an efficient simulation tool for the analysis of various phenomena. The two-scale model presented in this paper is benchmarked by a comparison of its numerical results with other models published in the literature. Several examples of microwave heating processes in various materials are simulated. Effects of heat-wave propagation in matter are predicted by the model. The results show the temporal and spatial evolution of the temperature and power-dissipation profiles. Variations in the (microwave) impedance profile in the medium due to the heating are computed. A further development of this model, including more complicated geometries and various loss mechanisms, may yield useful numerical tools for the synthesis and design of microwave heaters in which the heated material acts as a nonlinear load in the microwave circuit.**

***Index Terms*— Dielectric heating, dielectric thermal factors/ dielectric losses, electromagnetic heating (microwave heating), electromagnetic radiation effects (microwave radiation effects), resistance heating (electric heating).**

I. Introduction

COUPLED thermal-electromagnetic (EM) processes in temperature-dependent dielectric media are widely used in industrial application and in scientific experiments [1]–[3]. Numerical tools are needed in many such applications to simulate the interaction between the radiated medium (and its environment) and the microwave power. The simulation should take into account the temperature-dependent dielectric properties of the medium in order to solve the temporal and spatial evolution of the nonuniform temperature profile and the consequent distribution of the EM impedance.

Fig. 1 shows figuratively the microwave propagation through a medium with a complex, temperature-dependent dielectric permittivity $\varepsilon(T) = \varepsilon_o(\varepsilon'(T) - j\varepsilon''(T))$, where T is the local temperature. The heat generated by the microwaves inside the medium (through the dielectric losses presented by the imaginary component $\varepsilon''(T)$) is dissipated in a heat-conductivity process. The medium introduces a varying impedance profile for the incident wave and therefore acts as a nonlinear distributed load.

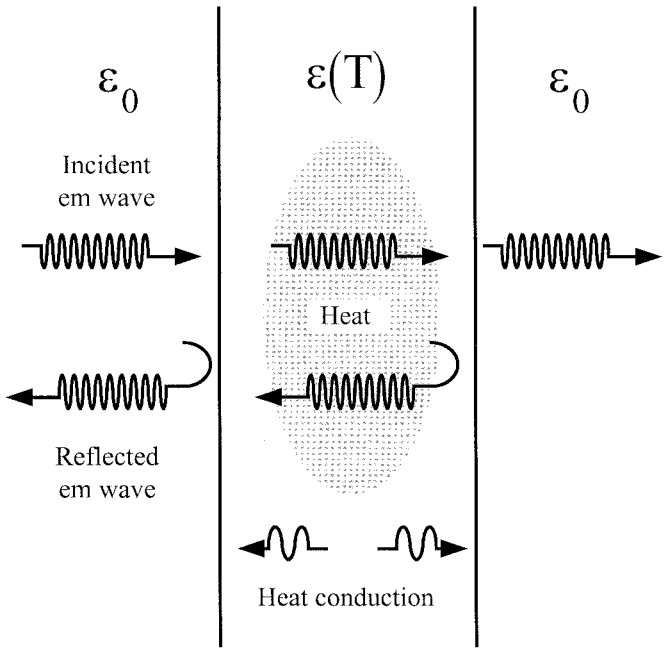

Fig. 1. A sketch of the coupled thermal-EM problem.

Coupled thermal-EM problems have been studied in the literature for various materials [4]–[14]. These include concrete [4], [5], Zirconia [6], Alumina [7], meat [8], water [9], SiC [10], [11], fat [12], and muscles [12]–[14]. These problems have been solved either by the finite-element method (FEM), or by the finite-difference time domains (FDTD) method. In the FEM, the structure is divided into an irregular grid, and the partial differential equations are solved by variational or residual methods. Solutions based on FEM are given for one-dimension [4], [15], two-dimension [5], [14], [16], and three-dimension [12], [17]–[19] configurations. In FDTD methods, the partial differential equations are substituted by a set of difference equations. FDTD methods have been used to solve two-dimension [7], [13], [20], [21] and three-dimension

Manuscript received September 4, 1998; revised December 10, 1998.

The authors are with the Department of Electrical Engineering and Physical Electronics, Faculty of Engineering, Tel-Aviv University, Ramat Aviv 69978 Israel.

Publisher Item Identifier S 0093-3813(99)04870-5.

[8], [10], [11], [20], [22] configurations. Ray-tracing methods are used for millimeter-wave heathing models [23].

Typically, three iterative steps are used to solve the coupling between the EM and thermal processes [4], [5], [7], [8], [10], [12], [13], [15]–[18]. First, the EM propagation in the medium is calculated. Then the power dissipation is evaluated using the local electric field. Finally, a thermal algorithm solves the time-dependent heat-diffusion equation and computes the new medium temperature profile. Generally, this process is repeated until some convergence criterion is satisfied. The inclusion of temperature-dependent dielectric properties produces a more accurate characterization of the coupled thermal-EM process [4], [6]–[8], [16], [18], [24].

Computer resources, such as run time and memory, limit the accuracy of thermal-EM simulations. For example, typical simulations needed more than 10 h of an HP730 workstation [8]. Faster programs required about a half hour of an IBM-3090 workstation [11]. In order to reduce the needs for these resources, algorithms use the diffused time-scale assumption. According to this assumption, the EM field attains a steady state [4], [5], [7], [8], [13], [16], [18], and therefore its time scale is much smaller than the heat diffusion. Other approximations reduce computation by temperature-distribution correction methods [7].

This paper analyzes microwave heating processes in temperature-dependent dielectric media subjected to microwave radiation. The model uses the FEM. Two different time scales are applied in order to reduce computation resources. Two separate diffusion functions are derived in order to simulate more accurately the localized temperature and the EM field distribution. This approach uses the linearity of the time-dependent heat-diffusion equation. It separates the thermal-EM problem into two independent solutions: one for heat-generation diffusion, and the other for the initial-temperature diffusion. The two equations are solved by accurate diffusion functions, which eliminate the field perturbation error rate [8], [18].

The model is derived in Section II. Numerical results are presented in Section III. A comparison with other models shows the validity of this model and its efficiency. Effects of heat wave propagation associated with the microwave heating process are predicted by the model.

II. Theory

A nonlinear model of microwave heating processes in dielectric media is derived in this section. The model includes temperature dependences of the dielectric properties which cause nonlinear effects and spatial nonuniformities in the heating process.

The problem solved by this model is sketched in Fig. 1. The dielectric material, in a form of a transversely infinite slab, is radiated by a perpendicular plane wave. Thermal boundary conditions, as well as impedance mismatch effects in the interfaces between the solid dielectric material and the air surrounding it, are included in the model. The model ignores material state-phase variations or any presence of liquids, vapors, or other materials inside the solid dielectric medium.

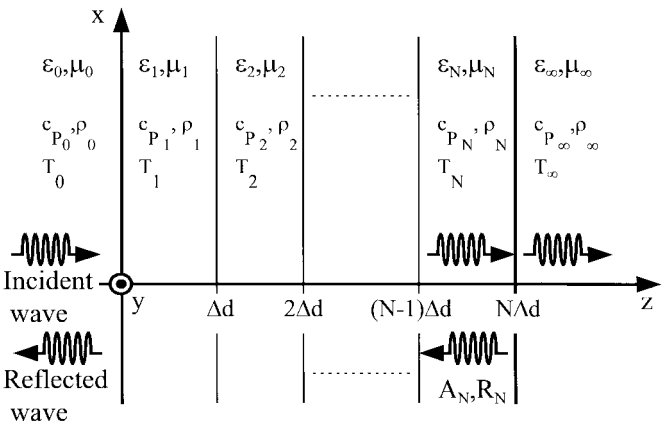

Fig. 2. A dielectric slab illuminated by an incident plane wave as a stratified layer model.

The local dielectric properties depend on the local temperature and on the EM frequency.

Different time scales are defined for the microwave propagation and for the temperature evolution in the medium. The propagation time of the EM wave is considered much shorter than the characteristic time of the temperature deviation in the medium. Thus, the temperature distribution is assumed to be steady during the propagation time of the EM wave along the medium. Consequently, the microwave heating process is separated into two coupled mechanisms in two iterative time scales. One is the EM-wave propagation time scale, and the other is the heat-diffusion time scale. The dominant mechanisms during these short and long time-scales, respectively, are described below.

A. Microwave Propagation

In order to analyze the wave propagation in the nonuniform medium, it is stratified by the model to thin layers as shown in Fig. 2. The dielectric permittivity of each infinitesimally thin layer may vary as a function of the local temperature, and it may depend on the instantaneous microwave frequency ω. The medium properties, such as the function $\varepsilon(T,\omega)$, are assumed to be known.

The EM plane wave propagates in the z direction, with perpendicular electric and magnetic field components $\vec{\boldsymbol{E}} = \hat{x}E_x(z,t)$ and $\vec{\boldsymbol{H}} = \hat{y}H_y(z,t)$, respectively. Following [25], the general solution of the one-dimension wave equation in the stratified medium is

$$E_n = A_n\left[e^{-j(k_n n z_n)} + \tilde{R}_{n,n+1}e^{-j(2k_n n\Delta d - k_n z_n)}\right] \qquad n\Delta d < z_n < (n+1)\Delta d \tag{1}$$

where E_n is the electric field in the nth layer, $k_n = \omega\sqrt{\mu_n\varepsilon_n}$ is the local wavenumber, A_n is the amplitude of the incident wave, $\tilde{R}_{n,n+1}$ is the overall reflection coefficient at the interface plane $z = n\Delta d$, and $R_{n,n+1}$ is the local reflection coefficient.

The values of A_n and $\tilde{R}_{n,n+1}$ are computed by continuity conditions between the various layers. The equations for the transmitted and reflected waves for the nth layer result in the

generalized reflection coefficient

$$\tilde{R}_{n,n+1} = \frac{R_{n,n+1} + \tilde{R}_{n+1,n+2} e^{-j2k_{n+1}\Delta d}}{1 + R_{n,n+1}\tilde{R}_{n+1,n+2} e^{-j2k_{n+1}\Delta d}}. \quad (2)$$

The amplitude A_n is related to A_{n-1} by

$$A_n = A_{n-1} S_{n-1,n} e^{-j(k_{n-1}-k_n)(n-1)\Delta d} \quad (3)$$

where the transfer relation for the nth layer is given by

$$S_{n-1,n} = \frac{1 + R_{n-1,n}}{1 + R_{n-1,n}\tilde{R}_{n,n+1} e^{j2k_n\Delta d}}. \quad (4)$$

The local reflection coefficient, i.e., the ratio between the reflected and incident wave amplitudes in the nth layer, is given by

$$R_{n,n+1} = \frac{E_n^r}{E_n^i} = \frac{\mu_{n+1}k_n - \mu_n k_{n+1}}{\mu_{n+1}k_n + \mu_n k_{n+1}} \quad (5)$$

where μ_n and k_n are the nth layer permeability and local wavenumber of the nth layer.

The EM field in the surface of the nth layer, $z = n\Delta d$, is given by

$$E_n = A_n\left[1 + \tilde{R}_{n,n+1}\right] e^{-jk_n n\Delta d}. \quad (6)$$

The EM power dissipation in each layer

$$\Delta Q_n = \frac{\omega}{2}\varepsilon_o \varepsilon_n'' |E_n|^2 \quad (7)$$

is the heat source in the coupled EM-thermal model as described below. The total power dissipated in the entire dielectric slab, i.e., the sum of all different layers

$$Q_0 = \sum_{n=1}^{N} \Delta Q_n \quad (8)$$

is used as an energy-conservation benchmark for the simulation accuracy.

B. Heat Transfer

A linear one-dimensional heat-conduction equation is given by

$$\frac{\partial T(z,t)}{\partial t} = \alpha \frac{\partial^2 T(z,t)}{\partial^2 z} + \frac{g(z,t)}{\rho c_p} \quad (9)$$

with the initial condition $T(z, t = 0) = T_0(z)$. The heat equation describes the evolution of the temperature distribution profile $T(z,t)$ in the medium, where $g(z,t)$ is the heat source distribution, α is the diffusion coefficient, ρ is the density, and c_p is the specific heat of the medium. The diffusion coefficient α may vary with the local temperature, as well as the other parameters in (9).

The temperature is divided in this model to two components, $T(z,t) = v(z,t) + w(z,t)$, where $v(z,t)$ satisfies the homogeneous heat equation

$$\frac{\partial v(z,t)}{\partial t} = \alpha \frac{\partial^2 v(z,t)}{\partial^2 z} \quad (10)$$

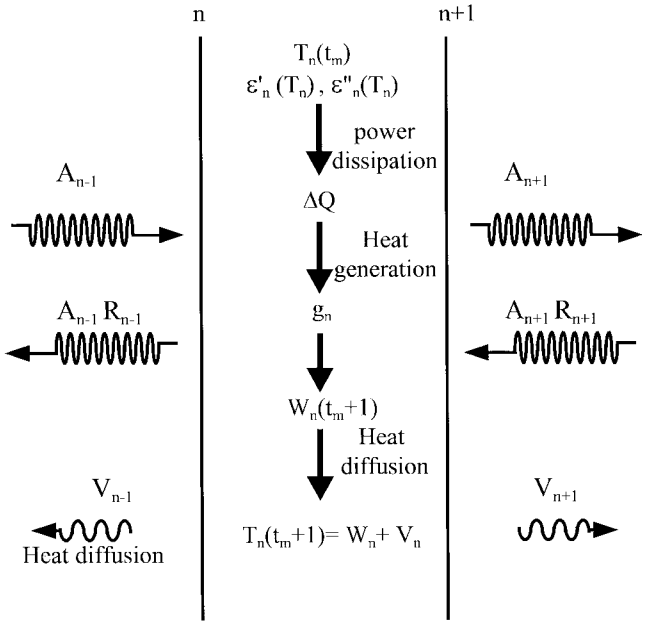

Fig. 3. The EM power transfer and heat-diffusion process in a single layer.

with the initial condition $v(z,0) = T_0(z)$, and $w(z,t)$ satisfies the inhomogeneous equation

$$\frac{\partial w(z,t)}{\partial t} = \alpha \frac{\partial^2 w(z,t)}{\partial^2 z} + \frac{g(z,t)}{\rho c_p} \quad (11)$$

with a null initial condition $w(z,0) = 0$. The heat diffusion and generation components in a single layer are shown schematically in Fig. 3.

The distinction between the functions v and w regards the temperature evolution as a combination of two processes in each iteration. The function v describes predominantly the heat diffusion, whereas the function w adds the heat generation process.

The solution for the initial-value problem, assuming that $\alpha(T)$ is constant only during the time interval Δt, is presented in the form [26]

$$v(z,t) = \int_{-\infty}^{\infty} K_v(z - \xi, \alpha t) T_0(\xi)\, d\xi \quad (12)$$

where the Kernel is given by

$$K_v(z, \alpha t) = \frac{1}{\sqrt{4\pi\alpha t}} e^{-\left(z^2/4\alpha t\right)}. \quad (13)$$

The solution for the inhomogeneous problem (11) is

$$w(z,t) = \int_{\xi=-\infty}^{\infty} \int_{\eta=0}^{\alpha t} K_w(\xi,\eta) \frac{g(z-\xi, \alpha t - \eta)}{\rho c_p}\, d\xi\, d\eta. \quad (14)$$

The time dimension is discretized in order to solve the coupled microwave-heating problem iteratively. The temperature distribution found in each iterative step is used as an initial condition for the successive step in (12). Assuming that the heat source is steady during the time interval Δt (i.e.,

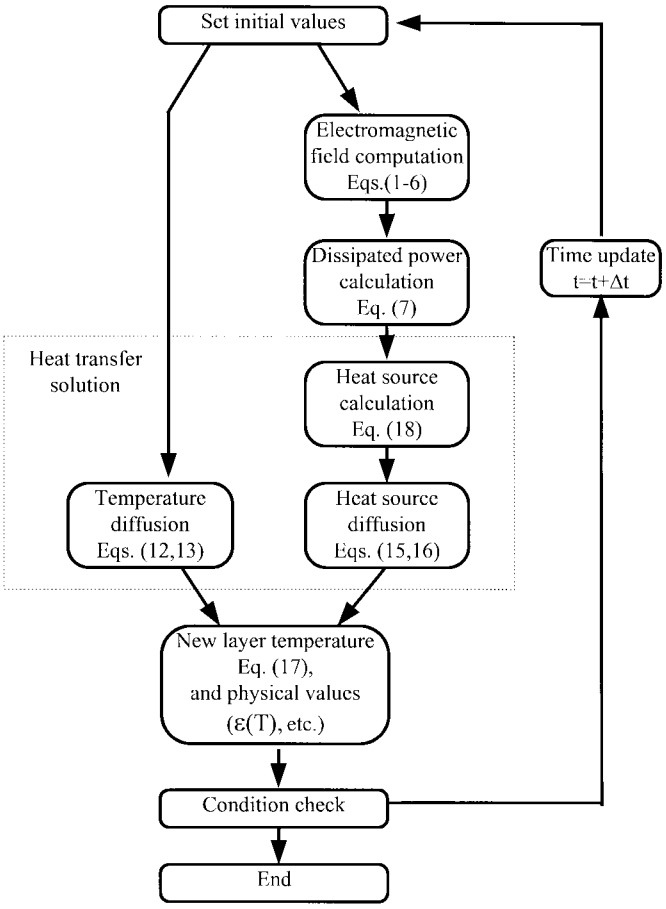

Fig. 4. A flow chart of the coupled thermal-EM model algorithm.

$g(z,t) = g(z,t_m)$ for $t_m < t < t_{m+1}$ where $t_m = m\Delta t$), the solution of (14) is given by

$$w(z,t) = \int_{\xi=-\infty}^{\infty} K_w(z-\xi, \alpha t_m) \frac{g(\xi, \alpha t_m)}{\rho c_p}\, d\xi \qquad t_m < t < t_{m+1} \tag{15}$$

where the heat-generation Kernel attains the form

$$K_w(z,\alpha t) = \int_{\eta=0}^{\alpha t} \frac{e^{-(z^2/4\eta)}}{\sqrt{4\pi\eta}} = \sqrt{\frac{\alpha t}{\pi}} e^{-(z^2/4\alpha t)} + \frac{z}{2}\left[\operatorname{erf}\left(\frac{z}{2\sqrt{\alpha t}}\right) - 1\right]. \tag{16}$$

The solution for the temperature during the time interval Δt is the discretized sum of the two independent effects [i.e., (12) and (25)] as follows:

$$T(z_n, t_m + \Delta t) = \sum_{n'=0}^{N+1} \left[K_v(z_n - n'\Delta d, \alpha t_m) T(n'\Delta d, t_m) + K_w(z_n - n'\Delta d, \alpha t_m) \frac{g(n'\Delta d, \alpha t_m)}{\rho c_p} \right]. \tag{17}$$

Boundary conditions are presented by dummy layers with specific properties in both sides of the finite rod, or by an adjustment of the heat source $g(z,t)$ value near the boundary layers.

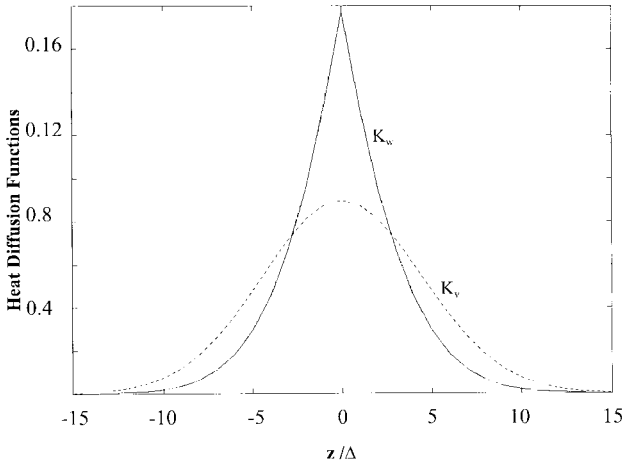

Fig. 5. The impulse-response temperature-diffusion functions K_v and K_w for concrete.

Assuming that there is no other heat energy source inside the medium (except the microwave radiation) the heat source $g(z,t)$ is given in any time interval at each layer by

$$g(z_n, t_m) = \Delta Q_n \Delta t = \frac{\omega \Delta t}{2} \varepsilon_o \varepsilon_n'' |E_n|^2. \tag{18}$$

Other processes, such as blackbody radiation and heat convection, can be included in the model by an adjustment of the heat source $g(z,t)$ parameter, as done in [7].

Each layer is characterized by parameters of diffusion coefficient, density, and specific heat. The microwave heat production ΔQ_n results in the evolution of the local temperature T_n. For the numerical simulation, (13) and (16) are discetized in space and time, and (17) is solved numerically. The expressions are used in Section III to simulate microwave heating processes in various conditions.

The computation process is described by a flow chart in Fig. 4. This two-scale method allows one to increase the time steps, hence to accelerate significantly the simulation run time. The normalized diffusion function results from the impulse response (13)

$$K_v(z,\alpha t) = \frac{1}{\sqrt{\pi}} \frac{1}{2\Delta} e^{-(z^2/4\Delta^2)} \tag{19}$$

where $\Delta = \sqrt{\alpha \Delta t}$ is shown in Fig. 5 with the function K_w.

The layer width (Δz) is taken to be smaller than 1/10 of the radiation wavelength. The width of the diffusion function (19) determines the typical time step for the computation as

$$\Delta t \sim \frac{4\Delta z^2}{\alpha}. \tag{20}$$

This time step is much longer than that used in any other method [4], [5], [7], [8], [22], and the computation time is much shorter accordingly. The blackbody radiation effect is not included yet in the model and therefore its validity is limited to ~300 °C. Numerical results are presented in Section III.

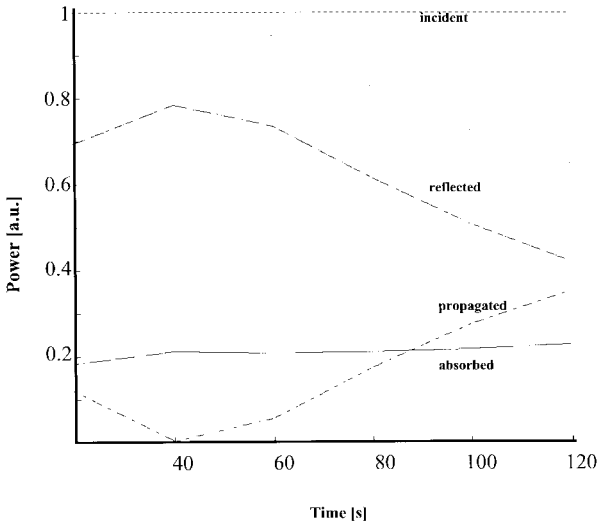

(a)

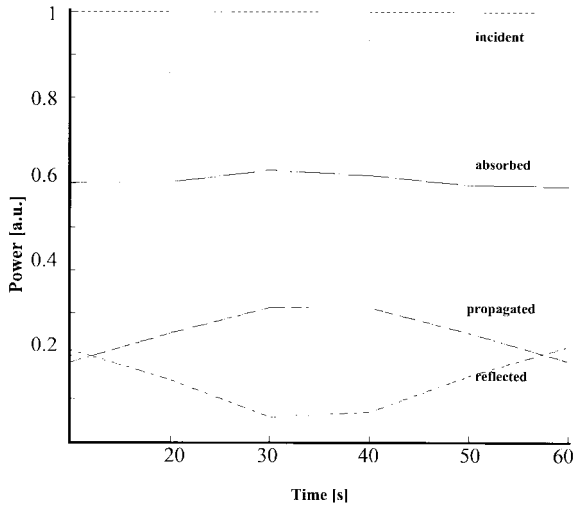

(b)

Fig. 6. Propagation and dissipation of microwave power in a concrete slab ($2.4 \cdot 10^6\ \mathrm{Wm}^{-2}$ along a 0.6-m slab) at (a) 0.896 GHz and at (b) 2.45 GHz.

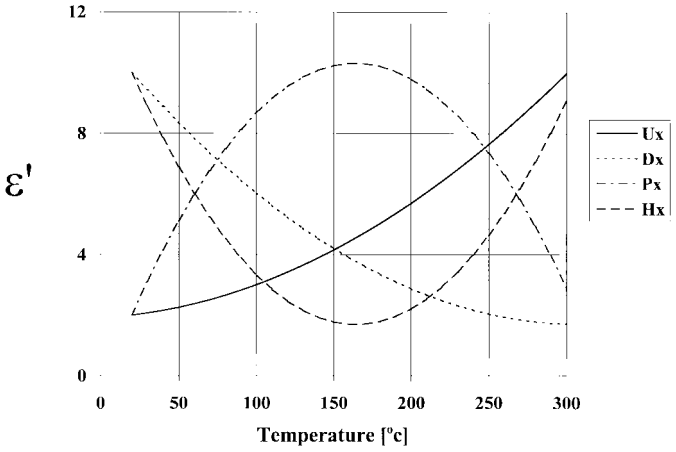

(a)

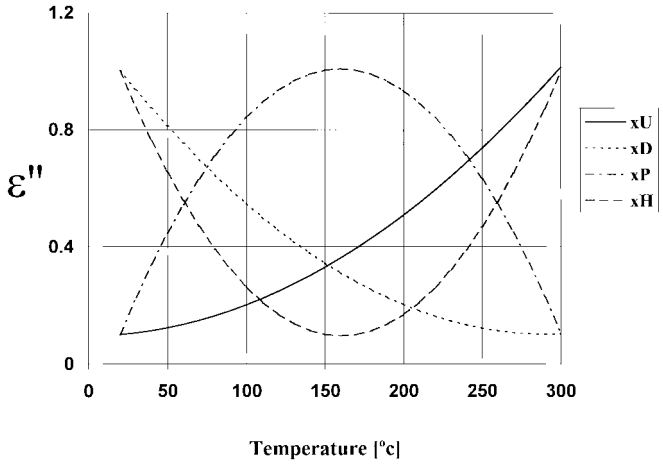

(b)

Fig. 7. Temperature dependences of dielectric permittivity components (a) $\varepsilon'(T)$ and (b) $\varepsilon''(T)$ for arbitrary materials chosen as examples for this analysis.

III. Results

Numerical results of the model are presented in this section in two aspects. First, published results of other models are used as a benchmark for the validity and computation time at the model. Second, the model is used to describe possible effects in materials with various (arbitrary) types of $\varepsilon(T)$ dependence. The code is applied as well to real materials such as Zirconia, Alumina, and food phantom based on parameters given in [6]–[8], respectively.

A. Comparison with Other Models

The results given in [4] are reproduced by our model. Both constant and temperature-dependent dielectric permittivities are compared. The computation was performed for each specified frequency (0.896, 2.45, 10.6, and 18.0 GHz). A regression process is computed in order to determine the dielectric-permittivity function on the basis of [4].

TABLE I
Temperature Dependence Types of Typical Materials' Dielectric Permittivities

Material	Frequency [GHz]	Temperature Range [°C]	Temperature Dependence	Ref.
Concrete	0.896	20-150	UU	[4]
	18.0	20-270	UU	
	10.6	20-270	UD	
	0.896	100-270	UP	
	2.45	150-270	UP	
	2.45	20-150	UH	
Zirconia	2.45	20-1100	UU	[6]
Alumina	2.45	20-1400	UU	[7]
Meat	2.45	12.5-48	DD	[8]
Water	2.45	10-100	DD	[9]

The power-dissipation at the high frequencies (10.6 and 18.0 GHz) in constant dielectric-permittivity values is perfectly matched to the results of [4]. In low frequencies, power-

TABLE II
PARAMETERS FOR THE ARBITRARY MATERIAL COMPUTATION

Thermal conductivity	1 $Wm^{-1}K^{-1}$
Thermal diffusitivity	10^{-6} $m^2 Scc^{-1}$
Total length	0.6 m
Frequency	2.45 MHz
Microwave power density	$2.4x10^5$ Wm^{-2}
Cell width	1.224 mm
Number of cells per wavelength	490
Time step interval	15 s

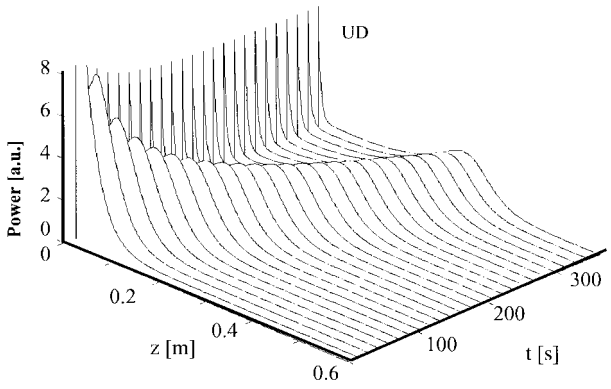

(a)

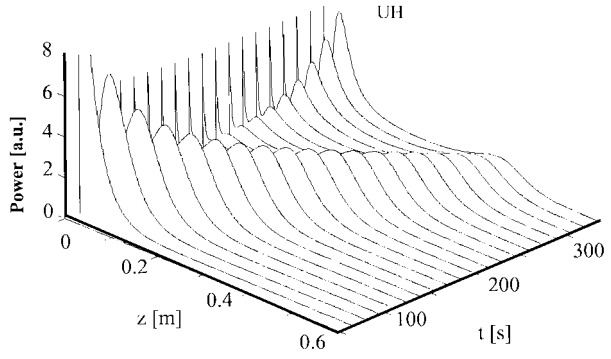

(b)

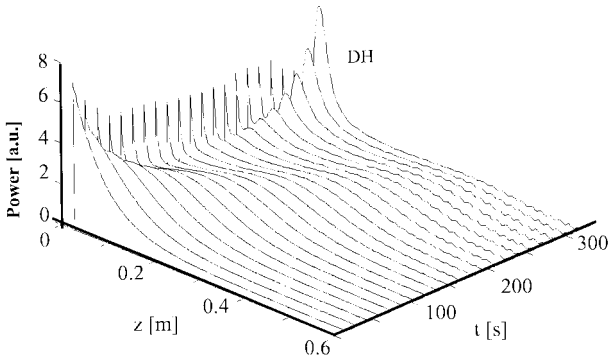

(c)

Fig. 8. The power-dissipation drift within arbitrary material types (a) UD, (b) UH, and (c) DH.

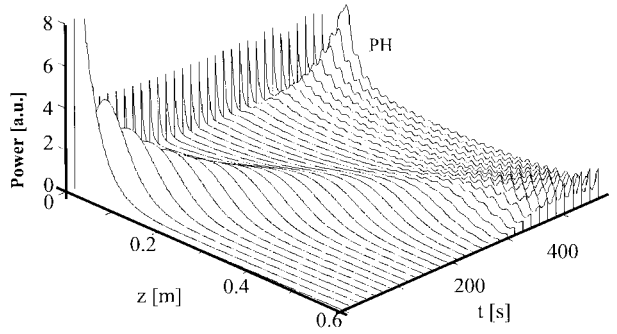

(a)

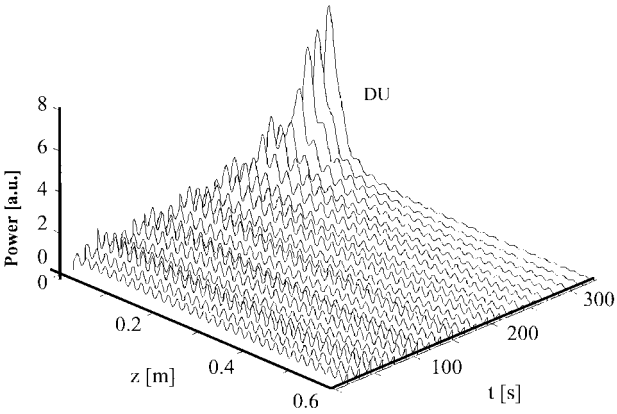

(b)

Fig. 9. The localized power dissipation within of the types (a) PH and (b) DU.

dissipation deviations of 10% at 2.45 GHz and 1.5% at 0.896 GHz are observed. Temperature distributions at high frequencies are matched within 0.5% deviation. At low frequencies, temperature distributions deviations of 10% at 2.45 GHz and 1% at 0.896 GHz are obtained. These mismatches are attributed to the surface-cooling effect and to the impedance mismatch effect. Both effects are included in our model but neglected in [4]. A full agreement of the temperature distribution results are accomplished by a power adjustment to the input level of [4].

The power dissipation and temperature distributions at high frequencies are also matched in the analysis of temperature-dependent dielectrics. Power-dissipation and temperature-distribution differences of less then 2 and 1%, respectively, are observed. At 2.45 GHz, differences of power dissipation within 12% and of temperature distributions within 3% are obtained (15 and 4%, respectively, at 0.896 GHz). An input power-level adjustment to compensate for the surface cooling results in a perfect agreement between the two models.

Fig. 6 shows the variations in the propagating, reflected, and absorbed microwave-power components during the heating process. The propagating power tends to increase at the beginning of the process and then decreases, whereas the reflected power has an opposite tendency. The absorbed power component remains almost constant. This nonlinear behavior of a temperature-dependent reflection coefficient is not described elsewhere in the literature.

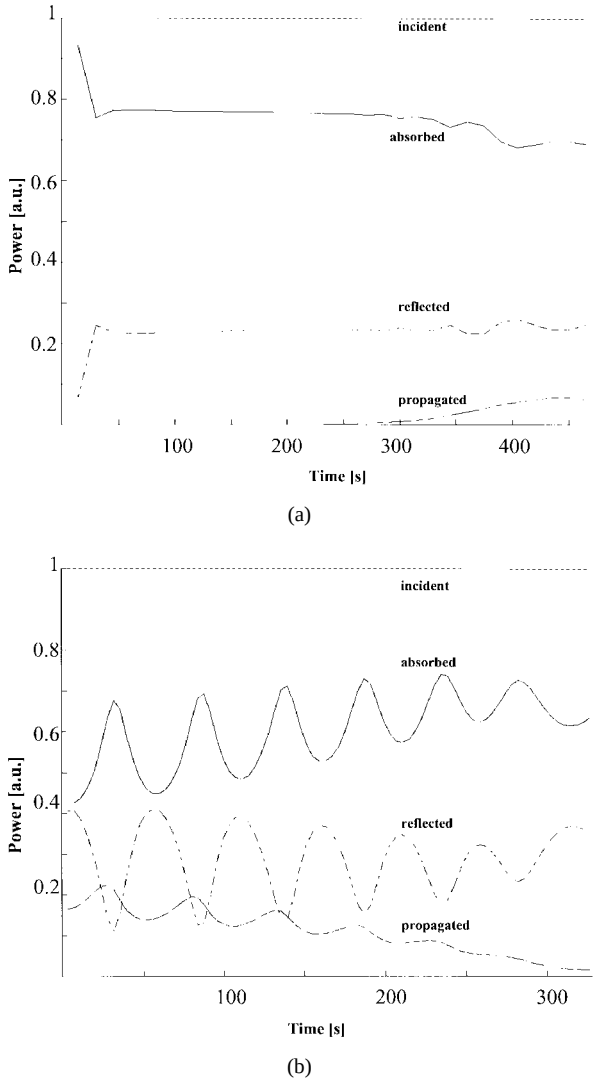

Fig. 10. Microwave power distribution within (a) PH and (b) DU materials, as in Fig. 9.

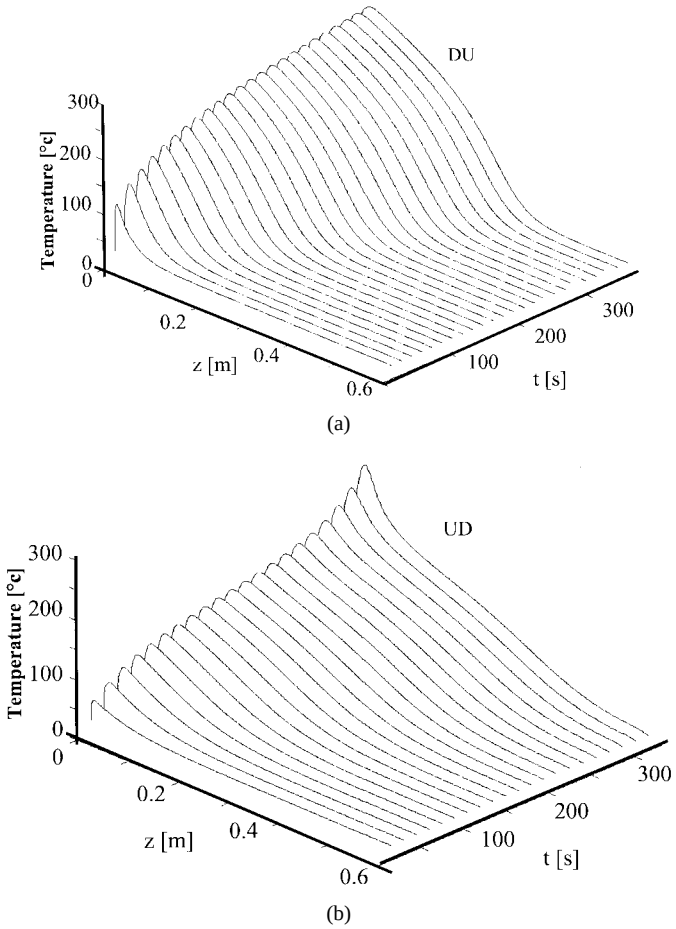

Fig. 11. Surface cooling and thermal runaway effects in (a) DH and (b) UD material types.

B. Results for Arbitrary Materials

In order to achieve a better understanding of the coupled thermal-EM phenomena, some arbitrary materials have been conceived. These arbitrary materials are characterized by different types of local temperature dependencies of the dielectric constant $\varepsilon'(T)$ and losses $\varepsilon''(T)$ as demonstrated in Fig. 7(a) and (b), respectively. The tendency of the temperature dependence is characterized by four groups, where U, D, P, and H denote "up," "down," "parabolic," and "hyperbolic" tendencies, respectively. Examples for real materials with temperature-dependent dielectric parameters are given in Table I. The other physical parameters used in this analysis are listed in Table II. The computation is terminated when the temperature reaches 300 °C. The parameters of this example were adjusted in order to yield the desired effects presented in this section.

A drift in the localized power concentration is observed in this analysis, as shown in Fig. 8(a)–(c). These effects, of a drifting localized power, are followed in some cases by a creation of a successive peak, as shown in Fig. 8(a) for UH material. A similar effect was observed also in DH, PH, and HH material types. Doubling the time and spatial resolutions yields the same phenomena. The heating rate plays a dominant role in this process, as will be presented in a future publication.

Another effect observed in this analysis in the oscillatory behavior of the penetrating power, shown in Fig. 9(a) and (b) and Fig. 10(a) and (b). This effect is observed in the media types UU, DU, DP, PU, PH, HU, HD, and HP. Heat oscillations observed were examined in different time and spatial resolutions. In the examination of Fig. 10(b), the same oscillations are obtained with time steps doubled twice (i.e., 1, 2, and 4). The "thermal-runaway" [9], [27] and "surface-cooling" phenomena are observed in this analysis, as demonstrated in Fig. 11(a) and (b).

IV. Discussion

A nonlinear model for heat-transfer and temperature-distribution evolution within media radiated by microwaves has been derived. The simulation run time and memory needs are reduced by using separate thermal-diffusion functions. The simulation examples provide a comparison with other models. These benchmarks prove the validity of the model and its efficiency and reveal the importance of new features embedded in it, such as the surface cooling and microwave impedance mismatch at the interface.

The analysis of power-dissipation and temperature distributions by this model reveals effects such as varying impedance distribution, local thermal-power drift, and power oscillation. The dynamic temperature-dependent reflection coefficient enables one to evaluate the microwave impedance variation and to increase the supplied power by an adaptive impedance matching apparatus. The temperature profiles predicted by the model provide a way to avoid thermal-runaway phenomena. The model is applicable also to combined temperature and frequency dependencies $(\varepsilon = \varepsilon(T, \omega))$ such as multifrequency heating mechanisms [28]. This model can be used to investigate the phenomena of heat oscillations and hot-spot drifts shown in Section III, and to study the effect of a varying heating rate. Advanced two-dimensional and three-dimensional versions of this model, including blackbody radiation, will be applicable to higher temperature ($>$300 °C) and to more complicated structures.

REFERENCES

[1] J. Thuery, *Microwaves: Industrial Scientific and Medical Aplications*. Boston, MA: Artech House, 1992.

[2] A. V. Gaponov-Grekhov and V. L. Granatstein, *Applications of High Power Microwave*. Boston, MA: Artech House, 1994.

[3] E. Jerby and M. Einat, "High-power microwaves—A useful tool in future industry," *Israel Energy News*, pp. 10–13, Winter 1997.

[4] W. Li, M. A. Ebadian, T. L. White, R. G. Grubb, and D. Foster, "Heat and mass transfer—In a contaminated porous concrete slab with variable dielectric properties," *Int. J. Heat Mass Transfer*, vol. 37, no. 6, pp. 1013–1027, Apr. 1994.

[5] L. E. Lagos, W. Li, M. A. Ebadian, T. L. White, R. G. Grubb, and D. Foster, "Heat transfer within a concrete slab with a finite microwave heating source," *Int. J. Heat Mass Transfer*, vol. 38, no. 5, pp. 887–897, Mar. 1995.

[6] R. Wroe and A. T. Rowly, "Evidence of a nonthermal microwave effect in the sintering of partially stabilized zirconia," *J. Mater. Sci.*, vol. 31, pp. 2019–2026, 1996.

[7] J. Clemens and C. Saltiel, "Numerical modeling of materials processing in microwave furnaces," *Int. J. Heat Mass Transfer*, vol. 39, no. 8, pp. 1665–1675, 1996.

[8] L. Ma, D. Paul, N. Pothecary, C. Railton, J. Bows, L. Barratt, J. Mullin, and D. Simons, "Experimental validation of a combined electromagnetic and thermal FDTD model of a microwave heating process," *IEEE Trans. Microwave Theory Tech.*, vol. 43, pp. 2565–2572, Nov. 1995.

[9] C. Vriezinga, "Thermal runaway and bistability in microwave heated isothermal slabs," *J. Appl. Phys*, vol. 79, pp. 1779–1783, Feb. 1996.

[10] Z. Huang, J. Tucker, and M. F. Iskander, "FDTD modeling of realistic microwave sintering experiments," *Proc. IEEE Antennas and Propagation Society Int. Symp.*, vol. 3, Seattle, WA, 1994, pp. 1798–1801.

[11] M. F. Iskander, R. L. Smith, O. Andrade, H. Kimery, and L. Walsh, "FDTD simulation of microwave sintering of ceramics in multimode cavities," *IEEE Trans. Microwave Theory Tech.*, vol. 42, pp. 793–799, May 1994.

[12] A. Sekkak, V. N. Kanellopoulos, L. Pichon, and A. Razek, "A thermal and electromagnetic analysis in biological objects using 3D finite elements and absorbing boundary," *IEEE Trans. Magn.*, vol. 31, pp. 1865–1868, May 1995.

[13] N. M. Pothecary and C. J. Railton, "A combined electromagnetic and thermal analysis of current sheet hyperthermia applicators," *Proc. 24th Europ. Microwave Conf. (EuMC)*, Cannes, France, 1994, pp. 625–629.

[14] G. T. Martin, M. G. Haddad, E. G. Cravalho, and H. F. Bowman, "Thermal model for the local microwave hyperthermia treatment of benign prostatic hyperplasia," *IEEE Trans. Biomed. Eng.*, vol. 39, pp. 836–844, Aug. 1992.

[15] D. Loyd, M. Karlsson, P. Ask, and B. E. Erlandson, "Hyperthermia of the prostate from a heat transfer point of view," *Proc. 16th Annu. Int. Conf. IEEE Engineering in Medicine and Biology Society*, vol. 2, Baltimore, MD, Nov. 1994, pp. 768–769.

[16] C. T. Choi and A. Konrad, "Finite element modeling of the RF heating process," *IEEE Trans. Magn.*, vol. 27, pp. 4227–4230, Sept. 1991.

[17] K. D. Paulsen, D. R. Lynch, and J. W. Strohbehn, "Three dimensional finite boundary and hybrid element solution of the Maxwell equation for lossy dielectric media," *IEEE Trans. Microwave Theory Tech.*, vol. 36, pp. 682–693, Apr. 1988.

[18] A. Sekkak, L. Pichon, and A. Razek, "3-D FEM magneto-thermal analysis in microwave ovens," *IEEE Trans. Magn.*, vol. 30, pp. 3347–3350, Sept. 1994.

[19] N. S. Goel and F. Gang, "A simple method for pulse-echo thermal wave imaging of arbitrary-shaped subsurface scatters in heterogeneous materials," *Int. J. Heat Mass Transfer*, vol. 23, pp. 45–54, Aug. 1996.

[20] N. S. Goel, Z. Ko, and F. Gang, "Electrostatic field in inhomogeneous dielectric media I. Indirect boundary element method," *J. Comput. Phys.*, vol. 118, pp. 180–188, 1995.

[21] I. S. Kim and W. J. R. Hoefer "A local mesh refinement algorithm for the time domain finite difference method using Maxwell's equations," *IEEE Trans. Microwave Theory Tech.*, vol. 38, pp. 812–815, June 1990.

[22] I. S. Zivanocic, K. S. Yee, and K. K. Mei, "A subgridding method for the time domain finite difference method to solve Maxwell's equations," *IEEE Trans. Microwave Theory Tech.*, vol. 39, pp. 471–479, Mar. 1991.

[23] L. Feher, G. Link, and M. Thumm, "The MIRA/THESIS 3D-code package for resonator design of millimeter-wave material processing," in *Proc. Symp. Microwave Processing of Materials V*, San Francisco, CA, Apr. 8–12, 1996.

[24] J. Jacob and L. H. L. Chia, "Review: Thermal and nonthermal interaction of microwave radiation with materials," *J. Mater. Sci.*, vol. 30, pp. 5321–5327, 1995.

[25] W. C. Chew, *Waves and Fields in Inhomogeneous Media*. New York: Van Nostrand Reinhold, 1990.

[26] J. R. Cannon, *The One-Dimensional Heat Equation*. California: Addison-Wesley, 1984.

[27] G. Roussy, A. Bennani, and J. M. Thiebaut, "Temperature runway of microwave irradiated materials," *J. Appl. Phys.*, vol. 62, pp. 1167–70, Aug. 1987.

[28] Y. Carmel, private communication.

Yaron Alpert was born in Israel in 1966. He received the B.Sc. degree in electrical engineering from Technion-Israeli Institute of Technology, Haifa, Israel, in 1993 and the M.Sc. degree (summa cum laude) in electrical engineering from Tel-Aviv University, Tel-Aviv, Israel, in 1999.

He works as an electrical engineer, specializing in communication. His research interests are numerical techniques for solving engineering problems, particularly related to microwave sources.

Eli Jerby, for a photograph and biography, see this issue, p. 293.